

## Searching for Anisotropy in Electron+Positron Cosmic Rays with CALET

---

Holger Motz<sup>\*</sup>, Yoichi Asaoka<sup>a</sup>, Shoji Torii<sup>a</sup> and Saptashwa Bhattacharyya<sup>b</sup>

*International Center for Science and Engineering Programs, Waseda University*

<sup>a</sup>*Research Institute for Science and Engineering, Waseda University*

<sup>b</sup>*Graduate School of Advanced Science and Engineering, Waseda University*

*E-mail: motz@aoni.waseda.jp*

The ISS-based Calorimetric Electron Telescope (CALET) is directly measuring the energy spectrum and direction distribution of electron+positron cosmic-rays up to 20 TeV. A main goal of CALET is to identify a signature of a nearby supernova remnant (SNR) in electron+positron cosmic-rays. The Vela SNR has the highest potential to cause a spectral feature in the TeV region and/or a detectable anisotropy. Using the numerical cosmic-ray propagation code DRAGON, the spectrum and expected anisotropy of the Vela SNR together with background from more distant SNR was calculated depending on injection and propagation conditions. The results of these calculations were used to simulate CALET event sky-maps on which several analysis methods were employed to estimate the CALET sensitivity. Assuming that there is no anisotropy, the expected limits on the dipole amplitude from an all-sky search were calculated as a function of the selected energy range and the shape of the predicted spectra. However for the detection of a dipole anisotropy, the direction towards Vela is predetermined, and sensitivity is strongly boosted by a directed search. It is shown that with this method, CALET has a significant probability to identify an anisotropy signature from Vela. As it may disturb the Vela signature, the contribution to the local cosmic-ray anisotropy from several other nearby SNR and pulsars, as well as from the general source distribution in the galaxy was studied. It was found that Vela is expected to dominate and have a detectable signature, though there is some influence from other sources on direction and strength of the anisotropy. Furthermore, the implications of detecting an dipole anisotropy directed towards Vela for the local propagation parameters, such as the diffusion coefficient, are explained.

*35th International Cosmic Ray Conference — ICRC2017*

*10–20 July, 2017*

*Bexco, Busan, Korea*

---

<sup>\*</sup>Speaker.

## 1. Introduction

The unknown electron + positron cosmic ray spectrum in the TeV region is expected to be dominated by cosmic rays emitted by nearby supernova remnants (SNR), since radiative energy loss limits the propagation distance of electron cosmic rays reaching Earth at TeV energy to less than one kiloparsec (kpc). The Vela SNR is a strong candidate for being the dominating source, due to its distance of 0.3 kpc and age of 11000 years. With one dominating source, a significant gradient in the cosmic ray density can be expected, causing an anisotropy in the measured flux.

## 2. Anisotropy Calculation with DRAGON

The expected anisotropy from the Vela SNR is derived by numerical cosmic-ray propagation calculation, which includes detailed effects such as energy losses, secondary particle production, and anisotropy of the diffuse background. DRAGON [1] features a non-equidistant spatial grid, allowing for a fine spatial binning near the observation point and sources required for calculation of anisotropy. The directional derivative of the cosmic ray density  $F(x,y,z)$ , is expressed as a difference between grid points with positions  $\vec{r}_1$  and  $\vec{r}_2$  on opposite sides of the Solar System's position  $\vec{r}_{sun}$ . The flux  $\Phi_{dir}$  from direction of the grid point at position  $\vec{r}_1$  is calculated as

$$\Phi_{dir} = \Phi_{avg} \left( 1 + \frac{3D(R)}{c} \frac{F(\vec{r}_1) - F(\vec{r}_2)}{|\vec{r}_1 - \vec{r}_2| F(\vec{r}_{sun})} \right) \quad (2.1)$$

where  $D(R)$  is the diffusion coefficient as a function of rigidity  $R$ . Using the  $9 \times 9 \times 9 = 729$  grid points in a cube up to 4 steps of 5 parsec away from the Solar System, the directional flux is calculated in 642 different directions, forming the dense mesh in galactic coordinates shown in figure 1. The predicted directional fluxes are then interpolated between these directions to fill a  $\approx 50k$  pixel HEALPix [2] map (nside = 64), and multiplied by the exposure of CALET (aperture  $1200 \text{ cm}^2 \text{ sr}$ , detection efficiency 90% [3]) to derive the expected events per pixel in CALET for five years of observation.

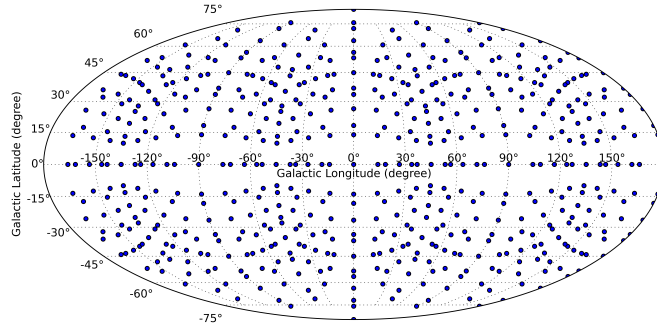


**Figure 1:** Map of the directions in which a directional flux is calculated with DRAGON

### 3. Model for Propagation of Cosmic Rays

The propagation model used in this study is based on the concepts from reference [4], updated to match more recent cosmic ray measurements including the positron excess. Furthermore numerical propagation calculation with DRAGON replaces analytical calculation. In the following, the chosen propagation conditions are described, resulting in the lepton and nuclei spectra shown in figure 2. A break in the diffusion coefficient has the potential to explain both the spectral hardening of the proton spectrum above 200 GV, as well as the change in the slope of the Boron to Carbon (B/C) ratio data[5]. A gradual change according to

$$D = D_0 \left( \frac{R}{R_0} \right)^{\delta_l} / \left( \frac{R}{R_b} \right)^{\frac{\delta_l - \delta_h}{s}} \quad (3.1)$$

is assumed, with  $\delta_l = 0.6$ ,  $\delta_h = 0.33$ ,  $R_0 = 4$  GV,  $R_b = 300$  GV,  $D_0 = 1.3 \cdot 10^{28}$  cm<sup>2</sup>/s, and a softness parameter  $s = 0.2$ . At 1 TeV, this parametrization gives  $D = 2.5 \cdot 10^{29}$  cm<sup>2</sup>/s. An injection power law index of  $\gamma_i = -2.92 + \delta_l = -2.32$  reproduces the AMS-02 [6] and CREAM [7, 8] proton spectrum measurements, and is used for all nuclei as well as electrons from distant and near SNR. Nearby PWN are assumed as the cause of the positron excess, of which Geminga (J0633+1746) and Monogem (J0659+1414) are regarded as dominating and included in the simulation using parameters from the ATNF catalogue [9]. The injection model assumes that the high energy electrons and positrons are confined in the PWN initially and released with the dissolving of the PWN after 40 kyr[10], with the injection flux exponentially decaying with a decay rate of 10 kyr[11]. The injection spectrum is a power law with exponential cut-off at 1 TeV and an index  $\gamma_{ip} = -1.8$ , chosen to match the AMS-02 data for positron flux [12] and positron fraction [13].

The four nearby SNR listed with their properties [14] in table 1 are simulated individually and each SNR's spectrum is normalized to a total output of  $1 \cdot 10^{48}$  erg in electron cosmic rays above 1 GeV. To investigate how delayed release of the electron cosmic rays from the SNR after the supernova affects the anisotropy signature, we calculate the spectrum for instantaneous release and constant release during a given period, as well as sudden release at a given time after the supernova explosion. The studied time ranges for both scenarios are 2500 yr, 5000 yr, 7500 yr and 10000 yr. A delayed release of the cosmic rays shifts the contribution from the Vela SNR and thus the possible anisotropy signature to higher energy as shown in figure 3. There is some deviation of the combined electron + positron spectrum from the measurement by AMS-02 [15], albeit in the range of the disagreement between this measurement and Fermi-LAT [16], and not decisive for an anisotropy study largely independent of the spectral shape.

SNR name	Longitude	Latitude	Distance [kpc]	Age [yr]
Cygnus Loop	74.0	-8.5	0.44	$2.0 \cdot 10^4$
Vela	263.9	-3.3	0.30	$1.1 \cdot 10^4$
Monogem	201.1	8.3	0.30	$8.6 \cdot 10^4$
Geminga	195.1	4.3	0.40	$3.4 \cdot 10^5$

**Table 1:** Properties of individually calculated nearby SNR

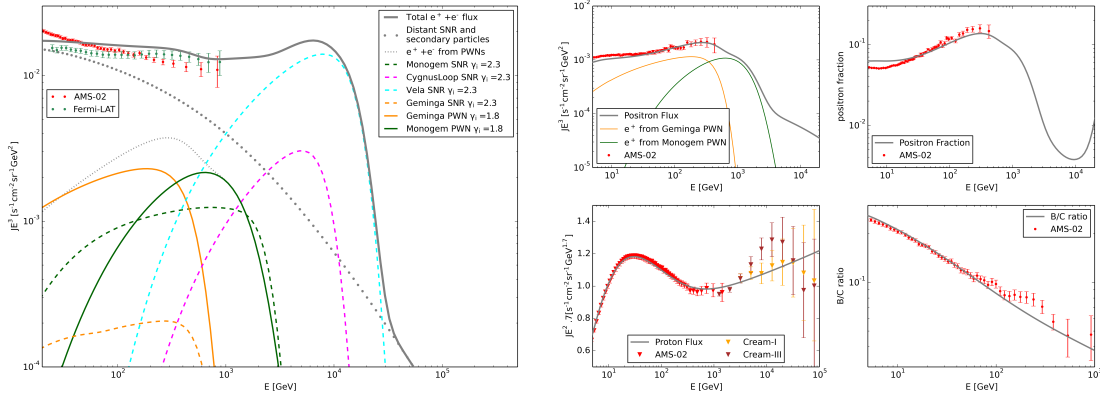


**Figure 2:** The electron + positron spectrum (left) and positron flux, positron fraction, proton flux and B/C ratio (right) from the DRAGON calculation, compared to experimental data.

#### 4. Expected Anisotropy in Electron+Positron Cosmic Rays

While the flux from the nearby SNR is absolutely normalized, the following other components of the spectrum are not absolutely normalized and are scaled to give the best fit to experimental data from AMS-02 by fitting in the energy/rigidity range of 20 - 1000 GeV/GV:

- the primary electron flux from distant SNR
- the primary nuclei flux and the secondary electron and positron fluxes linked to it
- the electron and positron flux from the PWNs are fitted with a common efficiency factor for conversion of rotational energy to cosmic rays

Applying the scales, the direction dependent expected event numbers in CALET from the resulting total electron + positron flux are calculated by the method described in section 2, integrating over all events above a given minimum energy  $E_{min}$ . From these maps, the expected anisotropy  $\frac{\Phi_{max} - \Phi_{min}}{\Phi_{max} + \Phi_{min}}$  is calculated using the anafast multipole analysis of the HEALPix package [2].

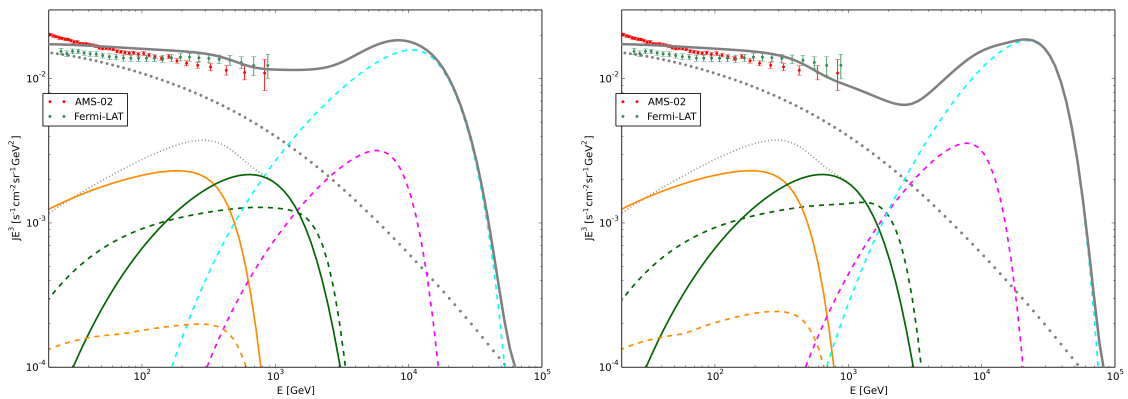


**Figure 3:** The electron + positron spectrum for release over a duration of 7500 years (left) and suddenly after 7500 years (right). For explanation of the spectrum components see figure 2.

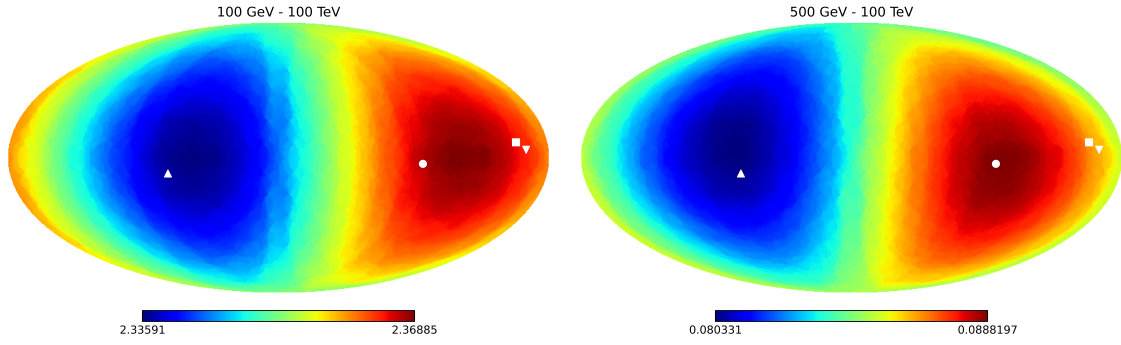


**Figure 4:** Anisotropy maps showing the expected number of events per pixel, for  $E > 100$  GeV (left) and  $E > 500$  GeV (right). The positions of nearby sources are shown by markers:  $\circ$  Vela (SNR),  $\square$  Monogem (SNR + PWN J0659+1414),  $\triangle$  Cygnus Loop (SNR),  $\nabla$  Geminga (SNR + PWN J0633+1746)

While Vela is the dominating in the TeV region, multiple sources determine the direction and strength of the anisotropy in the  $\approx 10^2$  GeV energy region. As demonstrated in figure 4, the contribution from Monogem and Geminga (SNR and PWN) shifts the anisotropy direction away from Vela at  $E_{min} = 100$  GeV, but for  $E_{min} = 500$  GeV, the dipole direction is centred on Vela. In general, the anisotropy rises with energy, due to the increase of both the contribution of individual SNR over the diffuse background, as well as the diffusion coefficient with energy. This is shown in figure 5 for the different cosmic ray release scenarios studied, compared to limits by Fermi-LAT [17, 18]. For release of the cosmic rays 7500 - 10000 years after the supernova, the anisotropy is strongly reduced at several 100 GeV, but rises in the TeV region. Though the anisotropy rises with energy, the optimal value of  $E_{min}$  to detect an anisotropy signature depends also on the number of detected events, which falls steeply with energy.

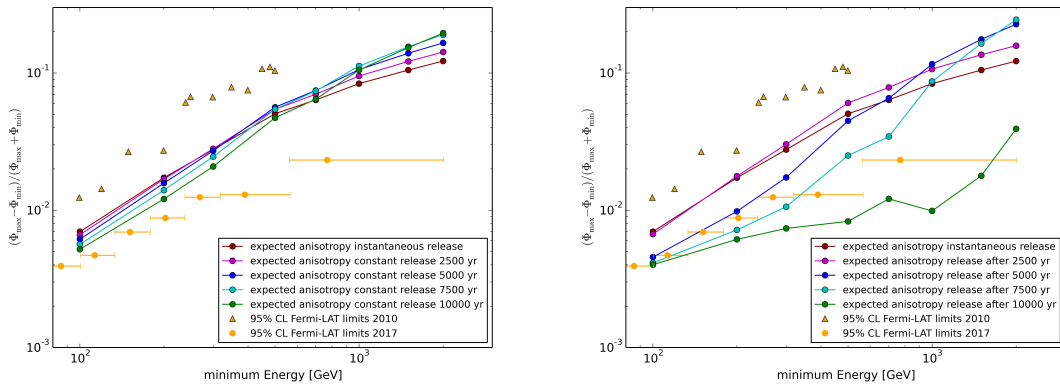


**Figure 5:** Expected anisotropy plotted against  $E_{min}$ , for cases of continuous injection of cosmic rays by SNRs (left), and for cases of delayed injection (right)

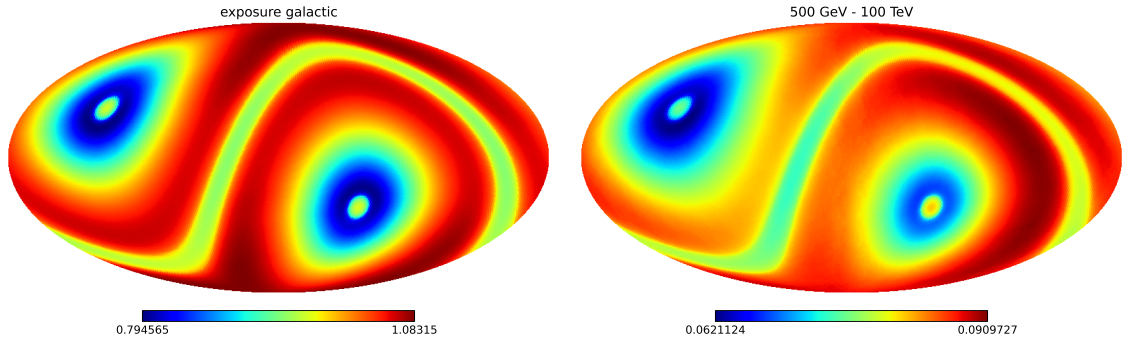


**Figure 6:** Left: Normalized exposure map ; right: Skymap of the expected events per pixel ( $E > 500$  GeV) from convolution of the exposure map with the map shown in figure 4 on the right

## 5. Simulation of Events in CALET

The exposure of CALET to the sky is not uniform but determined by the orbital parameters of the ISS and the acceptance angle of the detector. The geometrical requirements of event reconstruction give CALET a field of view up to a zenith angle of 45 degree. Based on this angle, a normalized exposure map in galactic coordinates was calculated using the orbital position of the ISS from October 2015 to April 2017, shown in figure 6. The skymaps of expected events per pixel obtained from simulations are convolved with this exposure map, giving the actual numbers of expected events taking the exposure to each sky region into account, with an example also shown in figure 6. Based on these skymaps of expected events convolved with the exposure map, 1000 samples of 5-year CALET data are simulated by drawing from the Poisson distribution to randomly determine the measured number of events in each pixel.

## 6. Expected CALET Limits on Anisotropy

For calculation of expected limits we follow the method described in reference [17], based on simulated samples created from a flat distribution of expected events over the sky convolved with the exposure map. Accordingly, in the analysis the simulated events are weighted with the exposure map as well, compensating this uneven distribution inherent to the measurement, but including the effect of non-uniform event density in the sensitivity estimation. Figure ?? shows the expected limits for the case of instantaneous cosmic ray release. These expected limits depend only on the number of events measured above  $E_{min}$ , thus they are comparable for all studied cases of cosmic ray release.

## 7. Expected Detection Probability for Anisotropy from Vela

While the calculated sensitivity for an all-sky-search indicates that no anisotropy from nearby SNR in the studied models could be detected, the possibility exists to detect an anisotropy from Vela with a fixed direction search. Due to the reduced number of degrees of freedoms, the significance of an excess in the predetermined direction would be significantly increased. With the

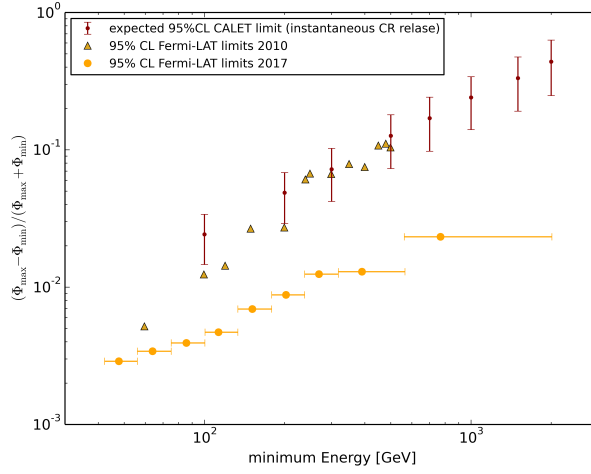


**Figure 7:** Expected anisotropy limit plotted against the minimum energy of the selected events.

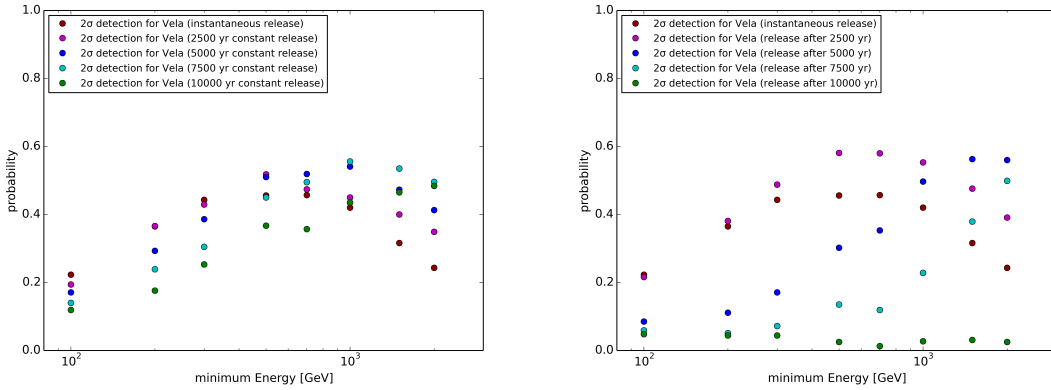


**Figure 8:** Probability of detecting anisotropy from the Vela SNR with CALET plotted against  $E_{min}$ , for cases of continuous injection of cosmic rays by all SNR (left), and for cases of delayed injection (right)

dipole direction fixed towards Vela, only the dipole magnitude is fitted to the simulated events, and a map for the expected event distribution created, including convolution with the exposure map. The likelihood  $P_{dipole}$  for this hypothesis is calculated as the product of the Poisson distribution probabilities for each pixel in the simulated event map, and compared to the likelihood  $P_{flat}$  for the base model, a flat distribution of events also convolved with the exposure map. The test statistics  $D = -2(\log(P_{flat}) - \log(P_{dipole}))$  follows a  $\chi^2$  distribution of one degree of freedom, with a critical value of 3.841 for  $2\sigma$  significance. The fraction of samples exceeding this critical value determines the detection probability shown in Figure 8 as a function of  $E_{min}$ . At which  $E_{min}$  the maximum probability occurs depends on the duration/time of the cosmic ray release, but a probability around 50% is reached for all cases except that of sudden release after 10000 years.

## 8. Conclusions and Outlook

- CALET is currently taking the first direct measurement of the TeV-region electron + positron flux, which could contain a signature from the Vela SNR, both in the spectrum and in the form of an anisotropy in the direction distribution of the events.
- The propagation model developed for this study can explain both the hardening of the proton spectrum around 200 GeV and the change in the slope of the B/C ratio by a soft break in the diffusion coefficient.
- A delayed release of the cosmic rays up to 10000 years after the supernova could create an anisotropy signature from Vela in the TeV region, while the already lower anisotropy in the  $\approx 10^2$  GeV region is further reduced by contributions from other nearby sources.
- Using a directed search towards Vela, CALET has some possibility to detect an anisotropy signature in almost all of the studied models.
- In case anisotropy is detected in the TeV region, the direct relation between anisotropy and the diffusion coefficient may allow to set lower bounds on the diffusion coefficient.
- Resolving the anisotropy caused by nearby SNR is a prerequisite to study the anisotropy signature related to the positron excess, where localised pulsar sources have to be discerned from a mostly flat emission from Dark Matter annihilation or decay.

## References

- [1] D. Gaggero, L. Maccione, G. Di Bernardo, C. Evoli, D. Grasso, *Phys.Rev.Lett.* **111**, 021102 (2013).
- [2] K. M. Górski, *et al.*, *Astrophys. J.* **622**, 759 (2005).
- [3] Y. Akaike, K. Kasahara, S. Torii, *International Cosmic Ray Conference* **6**, 371 (2011).
- [4] T. Kobayashi, Y. Komori, K. Yoshida, J. Nishimura, *Astrophys. J.* **601**, 340 (2004).
- [5] M. Aguilar, *et al.*, *Phys. Rev. Lett.* **117**, 231102 (2016).
- [6] M. Aguilar, *et al.*, *Phys. Rev. Lett.* **114**, 171103 (2015).
- [7] Y. S. Yoon, *et al.*, *Astrophys. J.* **728**, 122 (2011).
- [8] Y. S. Yoon, *et al.*, *Astrophys. J.* **839**, 5 (2017).
- [9] R. N. Manchester, G. B. Hobbs, A. Teoh, M. Hobbs, *Astron.J.* **129**, 1993 (2005).
- [10] D. Malyshev, I. Cholis, J. Gelfand, *Phys.Rev.* **D80**, 063005 (2009).
- [11] N. Kawanaka, K. Ioka, M. M. Nojiri, *Astrophys.J.* **710**, 958 (2010).
- [12] M. Aguilar, *et al.*, *Phys. Rev. Lett.* **113**, 121102 (2014).
- [13] M. Aguilar, *et al.*, *Phys. Rev. Lett.* **113**, 121101 (2014).
- [14] D. A. Green, *Bulletin of the Astronomical Society of India* **42**, 47 (2014).
- [15] M. Aguilar, *et al.*, *Phys. Rev. Lett.* **113**, 221102 (2014).
- [16] M. Ackermann, *et al.*, *Phys.Rev.* **D82**, 092004 (2010).
- [17] M. Ackermann, *et al.*, *Phys.Rev.* **D82**, 092003 (2010).
- [18] S. Abdollahi, *et al.*, *Phys. Rev. Lett.* **118**, 091103 (2017).